NeuroImage: Clinical 22 (2019) 101750

Contents lists available at ScienceDirect

NeuroImage: Clinical

journal homepage: www.elsevier.com/locate/ynicl

Altered brain tissue viscoelasticity in pediatric cerebral palsy measured by magnetic resonance elastography

Charlotte A. Chaze[a], Grace McIlvain[a], Daniel R. Smith[a], Gabrielle M. Villermaux[b], Peyton L. Delgorio[a], Henry G. Wright[c], Kenneth J. Rogers[d], Freeman Miller[d], Jeremy R. Crenshaw[e], Curtis L. Johnson[a,b,*]

[a] Department of Biomedical Engineering, University of Delaware, Newark, DE, United States
[b] Department of Psychological and Brain Sciences, University of Delaware, Newark, DE, United States
[c] Department of Physical Therapy, University of Delaware, Newark, DE, United States
[d] Department of Orthopedic Surgery, Nemours/A.I. duPont Hospital for Children, Wilmington, DE, United States
[e] Department of Kinesiology and Applied Physiology, University of Delaware, Newark, DE, United States

ARTICLE INFO

Keywords:
Cerebral palsy
Magnetic resonance elastography
Stiffness
Brain
Pediatric
Viscoelasticity

ABSTRACT

Cerebral palsy (CP) is a neurodevelopmental disorder that results in functional motor impairment and disability in children. CP is characterized by neural injury though many children do not exhibit brain lesions or damage. Advanced structural MRI measures may be more sensitively related to clinical outcomes in this population. Magnetic resonance elastography (MRE) measures the viscoelastic mechanical properties of brain tissue, which vary extensively between normal and disease states, and we hypothesized that the viscoelasticity of brain tissue is reduced in children with CP. Using a global region-of-interest-based analysis, we found that the stiffness of the cerebral gray matter in children with CP is significantly lower than in typically developing (TD) children, while the damping ratio of gray matter is significantly higher in CP. A voxel-wise analysis confirmed this finding, and additionally found stiffness and damping ratio differences between groups in regions of white matter. These results indicate that there is a difference in brain tissue health in children with CP that is quantifiable through stiffness and damping ratio measured with MRE. Understanding brain tissue mechanics in the pediatric CP population may aid in the diagnosis and evaluation of CP.

1. Introduction

Cerebral palsy (CP) is a neurodevelopmental disorder that results in functional motor impairment and disability in children (Bax, 1964; Bax et al., 2005) and affects over 800,000 children and adults in the US (Krigger, 2006). Brain tissue lesions and malformations in CP are thought to be the underlying cause of impairment (Himmelmann et al., 2017), but CP is predominately diagnosed based on the primary symptom of motor impairment and many children diagnosed with CP show no defects or lesions in their structural MRI scans (Himmelmann et al., 2017). In recent years, the diagnosis and management of CP in children has witnessed a growing reliance on advanced neuroimaging methodologies (Gosling, 2017). Neuroimaging techniques such as functional MRI, MR spectroscopy, and diffusion tensor imaging can identify neural damage that affects motor performance (Korzeniewski et al., 2007; Nagae et al., 2007; Thomas et al., 2005) and have contributed to the characterization of brain health in children with CP. These advanced imaging techniques have the potential to improve diagnosis and evaluation of CP, describe specific patterns of brain injury and malformation that contribute to functional impairments in children with CP, and monitor neuroplastic response to rehabilitation (Aisen et al., 2017).

Magnetic resonance elastography (MRE) (Manduca et al., 2001; Muthupillai et al., 1995) is a quantitative imaging technique that may provide an additional neuroimaging approach to characterize brain health in CP. MRE noninvasively assesses brain tissue viscoelastic mechanical properties, such as stiffness and damping ratio, which act as measures of neural tissue integrity (Hiscox et al., 2016; Murphy et al., 2017; Sack et al., 2013). Previous studies have demonstrated that these properties vary with age in adults (Arani et al., 2015; Hiscox et al., 2018), between normal and disease states (ElSheikh et al., 2017; Fehlner et al., 2016), and are related to cognitive function (Johnson et al., 2018; Schwarb et al., 2016). The use of brain MRE to study the mechanical properties of the pediatric brain is limited, with the first

* Corresponding author at: 150 Academy St, Newark, DE 19716, United States.
E-mail address: clj@udel.edu (C.L. Johnson).

https://doi.org/10.1016/j.nicl.2019.101750
Received 29 August 2018; Received in revised form 15 February 2019; Accepted 5 March 2019
Available online 07 March 2019

measurements of adolescent brain viscoelasticity only recently reported (McIlvain et al., 2018), despite the high potential for MRE to sensitively characterize brain health in neurological conditions affecting children (Johnson and Telzer, 2018). Using MRE to quantify brain tissue viscoelastic properties as physiological biomarkers associated with CP could elucidate the origin and severity of motor impairment in this population.

In this study, we used MRE to examine children with CP compared to typically-developing (TD) children. We hypothesized that children with CP will have reduced mechanical integrity of the brain representative of the neurological damage that results in clinical disability. We considered differences in mechanical properties between groups both globally and regionally through a voxel-wise analysis to identify regions affected by CP. This is the first study to examine CP with MRE and one of the first to apply MRE to studying the pediatric brain.

2. Methods

2.1. Participants

We enrolled children 5–12 years old for this study, which included an MRI scan (described below) and a functional assessment to characterize disability from CP using the Gross Motor Function Classification System (GMFCS). These sessions were separated by no more than one week. All children provided assent and guardians provided consent for participation in this study approved by our Institutional Review Board. 12 children (7 female, 5 male) with spastic CP were recruited through the orthopedic surgery clinic at Nemours/A.I. duPont Hospital for Children, along with 11 TD children (6 female, 5 male) recruited from the surrounding community as control participants. Two children with CP had enlarged ventricles, presumably from periventricular leukomalacia (PVL), and were excluded from group analyses. Thus, the total number of participants included in group analyses was 21 (10 CP, mean age 8.1 years; 11 TD, mean age 8.8 years). The participants with CP had a GMFCS disability score of 1 ($N = 7$) or 2 ($N = 3$), representing the lowest levels of impairment in CP.

2.2. Magnetic resonance elastography

MRI scans were completed using a Siemens 3 T Prisma scanner and 20-channel head RF-receive coil. The imaging protocol included MRE and additional anatomical scans. The entire protocol was limited to 20 min to maximize compliance as children were not sedated for the imaging session. Additionally, we used an MR-compatible goggle system (VisuaStimDigital; Resonance Technology, Inc.; Northridge, CA) to show participants a movie of their choice throughout the entire session.

MRE data were collected using a single-shot EPI sequence with the following imaging parameters: FOV = 240 × 240 mm^2; matrix = 96 × 96; 48, 2.5 mm thick slices; TR/TE = 6720/69 ms; GRAPPA $R = 3$; final resolution = 2.5 × 2.5 × 2.5 mm^3. A pneumatic driver system (Resoundant, Inc.; Rochester, MN) delivered vibrations to the head at 50 Hz. Four phase offsets were acquired in a total scan time of 3 min 15 s. Complex displacement fields were created from MRE images following phase unwrapping with FSL PRELUDE (Jenkinson, 2003) and temporal Fourier filtering. Viscoelastic shear stiffness property maps were generated from MRE displacement images using a nonlinear inversion (NLI) algorithm (McGarry et al., 2012). NLI returned property maps of the complex viscoelastic shear modulus $G^* = G' + iG''$, where G' and G'' are the storage and loss moduli, respectively. Viscoelastic shear stiffness, μ, was calculated as $\mu = \frac{2|G^*|^2}{G'+|G^*|}$ (Manduca et al., 2001), and damping ratio, ξ, was calculated as $\xi = \frac{G''}{2G'}$ (McGarry and Van Houten, 2008). Fig. 1 shows an overview of the MRE procedure and mechanical property measures.

2.3. Global analyses

A priori region-of-interest (ROI) analysis included ROIs of bilateral cerebrum, cerebral white matter (WM), and cerebral gray matter (GM). FSL FAST (Zhang et al., 2001) was used to segment anatomical images into WM and GM masks in native space for each subject. Bilateral cerebral masks from the WFU PickAtlas (Maldjian et al., 2003) were then registered to MRE native space. Atlases were applied to the shear stiffness and damping ratio maps for each subject to isolate ROIs of the cerebrum. The average stiffness and damping ratio of each ROI was calculated for each participant in the CP and TD groups, and one-way ANOVAs were used to test for differences in cerebral viscoelasticity between groups for each region and property separately.

2.4. Voxel-wise analyses

A data-driven approach using voxel-wise statistics was performed to investigate focal differences in brain tissue mechanical properties between CP and TD groups. First, shear stiffness and damping ratio property maps were registered to standard MNI space at 2.0 mm resolution using FSL FLIRT (Jenkinson et al., 2002; Jenkinson and Smith, 2001). To compare each voxel between the two groups, a one-way ANOVA was performed on each voxel individually across the brain. This analysis was performed for stiffness and damping ratio separately.

To overcome the challenge of characterizing error rates from multiple comparisons for a voxel-wise MRE analysis, we used an estimation of the false discovery rate (FDR) (Benjamini et al., 1995). Specifically, we used the linear step-up (LSU) procedure created by Simes (Simes, 1986) and developed in detail by Benjamini-Hochberg (Benjamini et al., 1995). This procedure ranks the p-values from each individual test in order from smallest to largest and assigns the smallest with rank $i = 1$, the next $i = 2$, and so on. Each p-value is compared to its Benjamini-Hochberg critical value, $(i/m)Q$, where i is the rank, m is the total number of tests, and Q is the chosen FDR. The test with the largest

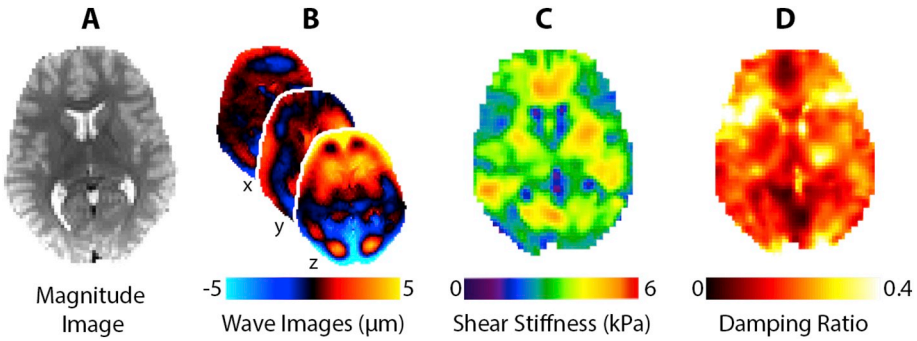

Fig. 1. Overview of the MRE procedure using a representative participant. A) Anatomical MRE magnitude image; B) wave images at 50 Hz showing displacements in the x, y, and z directions; C) shear stiffness map and D) damping ratio map calculated from displacement fields.

p-value where $p < (i/m)Q$ is assigned as significant, and all of the tests with p-values smaller than it are also significant (including the ones that aren't less than their Benjamini-Hochberg critical value). This procedure has been proven to control the FDR both under the assumption of independence between p-values and under a positive dependence assumption. Using this method, we control the proportion of false positive voxels to the voxels that are labelled as showing significant differences between groups. We removed all voxels with FDR > 0.05, which allows us to assume that each significant voxel has at most a 5% chance of being a false positive. The five largest clusters of voxels were then identified based on their voxel volume and were located anatomically based on their cluster centroids.

3. Results

Fig. 2 presents example stiffness and damping ratio maps from our population, including a TD participant, a CP participant, and a CP participant exhibiting PVL, a type of brain damage common in CP (Robinson et al., 2009). The CP subject with PVL shows an enlarged left ventricle taking over much of the periventricular WM space and the stiffness and damping ratio maps are influenced by this abnormal ventricle. Only two participants in our sample exhibited these enlarged ventricles and they were excluded from the group analyses.

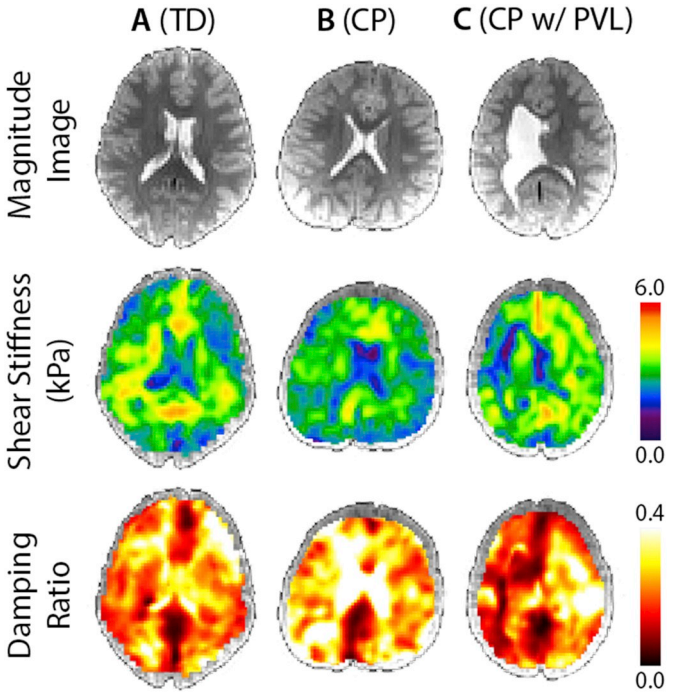

Fig. 2. Magnitude images, stiffness maps, and damping ratio maps in neurological convention for A) a typically developing (TD) subject; B) a subject with cerebral palsy (CP); and C) a subject with CP who also displays periventricular leukomalacia (PVL).

Fig. 3A and Table 1 present the stiffness of each global ROI for both CP and TD groups. The CP group had lower stiffness in each global ROI with medium-to-large effect sizes for each regional comparison; however, this difference was only significant in the GM region ($p < .05$). Fig. 3B and Table 2 additionally present the global damping ratio statistics for each group. The CP group exhibited higher damping ratio, again with medium-to-large effect sizes in each ROI, though with the whole cerebrum and GM being significantly different between groups ($p < .05$). The CP group had, on average, 6.0% lower GM stiffness and 6.5% higher damping ratio than the TD group. Tables S1 and S2 present the storage and loss moduli, G' and G'', for each ROI for both groups. The storage modulus shows a larger difference between groups indicating that the lower stiffness and higher damping ratio may be attributed to reduced tissue elasticity.

Table 1
Descriptive statistics for stiffness of each global ROI in both CP and TD groups (mean ± standard deviation), p-value, F-statistic, and η^2 effect size for each comparison between groups.

		Shear stiffness (kPa)	p	$\|F\|$	η^2
Cerebrum	CP	2.79 ± 0.13	0.067	3.78	0.166
	TD	2.89 ± 0.12			
White matter	CP	2.90 ± 0.13	0.259	1.36	0.066
	TD	2.97 ± 0.12			
Gray matter	CP	2.65 ± 0.15	0.015	7.19	0.275
	TD	2.82 ± 0.13			

Table 2
Descriptive statistics for damping ratio of each global ROI in both CP and TD groups (mean ± standard deviation), p-value, F-statistic, and η^2 effect size for each comparison between groups.

		Damping ratio	p	$\|F\|$	η^2
Cerebrum	CP	0.250 ± 0.011	0.048	4.45	0.190
	TD	0.238 ± 0.015			
White Matter	CP	0.251 ± 0.010	0.188	1.87	0.089
	TD	0.243 ± 0.015			
Gray Matter	CP	0.247 ± 0.013	0.032	5.35	0.220
	TD	0.232 ± 0.015			

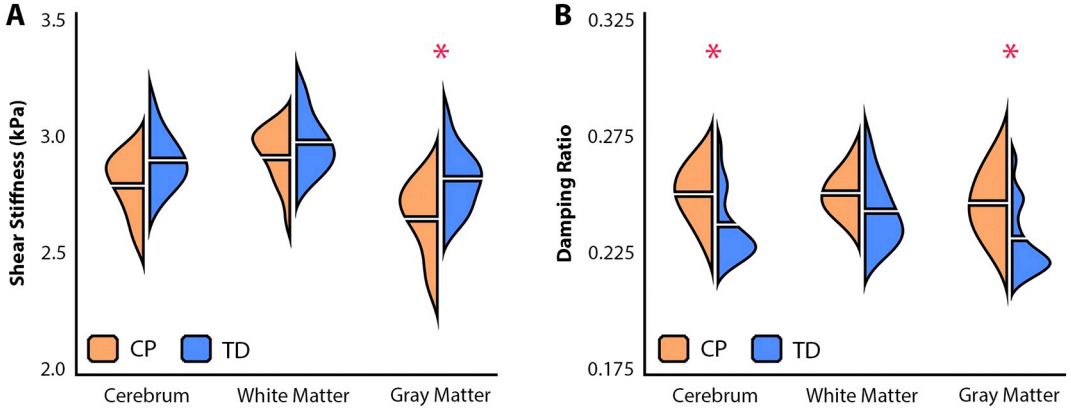

Fig. 3. Bean plots illustrating A) stiffness values and B) damping ratio values for CP and TD groups in each ROI. The horizontal break on either side of each bean represents the group mean. Significant differences between groups ($p < 0.05$) marked by *.

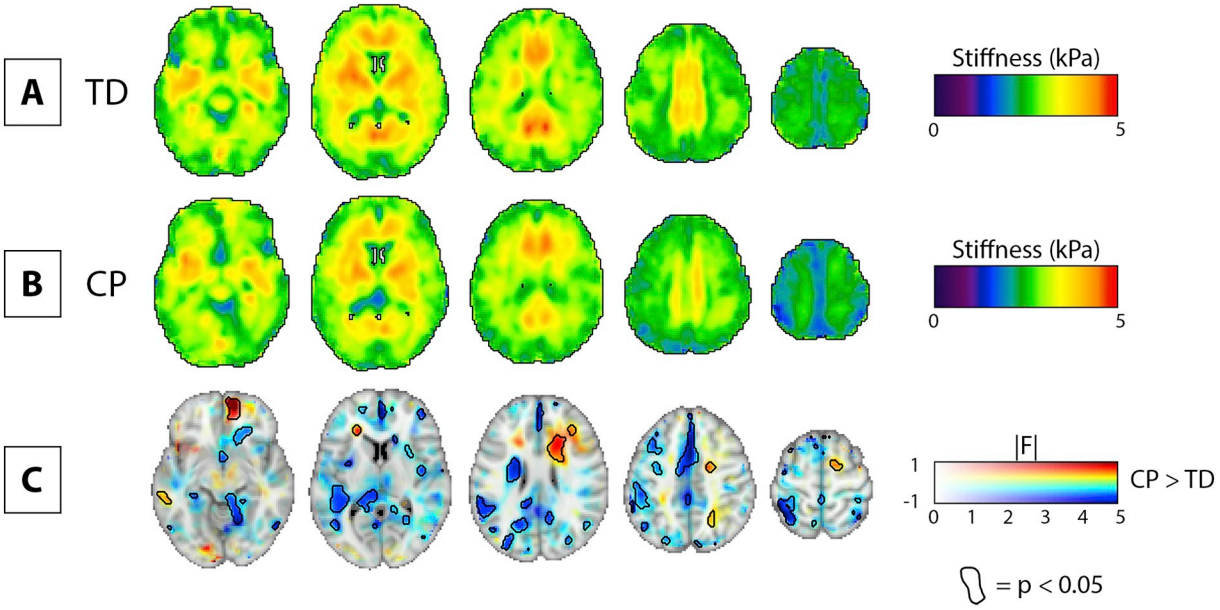

Fig. 4. Voxel-wise comparison of stiffness between TD and CP groups. A) Example slices of the mean stiffness map for TD group. B) Example slices of the mean stiffness map for CP group. C) Multidimensional statistical map including the voxel-wise CP > TD difference map as a colored feature plane; the associated F-statistics in opacity; and areas where $p < 0.05$ circled. 2.0 mm MNI standard-space template underlay for visualization. All images in neurological convention.

Group averaged stiffness maps in standard space are shown for the TD group and the CP group in Fig. 4A and B. Fig. 4C illustrates the voxel-wise CP > TD difference map, with magnitude of difference represented with color and associated F-statistics represented in opacity. Areas with significant difference between groups ($p < .05$) are circled in black. Fig. 4C is designed according to the neuroimaging data visualization recommendations suggested by Allen et al. (2012).

We identified clusters of voxels exhibiting significant stiffness differences between groups. The volume (number of voxels) and cluster centroid location in MNI coordinates of the five largest significant clusters in the CP > TD difference map are described in Table 3. These large clusters are situated in the left limbic, temporal, parietal, and frontal lobes, and in the right sub-lobar region. These large clusters generally expressed significantly lower stiffness in CP, though one area was significantly stiffer in CP (cluster 5 in Table 2, right sub-lobar).

We additionally performed a voxel-wise analysis on damping ratio between groups, with group-averaged properties and difference maps presented in the same format as the stiffness comparison (Fig. 5). We similarly found clusters of significant voxels with size and location collected in Table 4. These regions were in the left parietal and frontal lobes and sub-lobar region, with the largest clusters exhibiting higher damping ratio in CP.

4. Discussion

In this work, we analyzed the mechanical properties of the brain in children with CP. Overall, we found the brains of children with CP to be less stiff and have higher damping ratio than TD children, particularly in GM, and that patterns of lower stiffness and higher damping ratio in both GM and WM were found throughout the brain via voxel-wise analysis. Based on previous observations using MRE in studying neurodegenerative conditions in the adult brain (Hiscox et al., 2016; Murphy et al., 2017), the lower brain stiffness may be indicative of reduced structural integrity of brain tissue in CP. The higher damping ratio is potentially related to functional impairment and clinical outcomes in CP, as this measure has been previously related to memory function and fluid intelligence (Johnson et al., 2018; Schwarb et al., 2016).

The degree of motor impairment in children with CP can be categorized through the GMFCS. The GMFCS is a 1–5 scale based on movements including sitting, walking, and use of mobility devices. In this study, seven CP participants had a score of 1 and three CP participants had a score of 2. These GMFCS scores represent the lowest levels of functional motor impairment from CP. Notably, we still found significant differences in stiffness and damping ratio of GM between the CP group and the TD group, indicating that even at the lowest levels of cognitive and motor impairment, MRE is a valuable tool for analysis of this population. We expect that children with greater levels of impairment (*i.e.* higher GMFCS scores) may exhibit further reduced stiffness. Despite the limited sample in this study, the two participants at GMFCS 2 – both males, 6 and 10 years old – did indeed exhibit lower cerebral stiffness than the overall CP group (average = 2.71 kPa) and higher cerebral damping ratio (average = 0.259). Future work may build on this preliminary data to examine children with CP and greater functional impairment.

Two of the CP subjects exhibited PVL (Fig. 2C), a type of brain

Table 3
The five largest clusters of voxels in 2 mm standard space exhibiting significant differences in stiffness between groups as identified through voxel-wise analysis. MNI coordinates identify the location of the cluster centroid. Note all clusters show significantly lower softness in CP except for cluster 5, which shows higher stiffness.

Cluster	# Voxels	MNI coordinates	Anatomical location
1	4603	(−3, −61, 28)	Left Cerebrum//Limbic Lobe//Cingulate Gyrus
2	1516	(−60, −19, −6)	Left Cerebrum//Temporal Lobe//Middle Temporal Gyrus
3	1297	(−63, −33, 37)	Left Cerebrum//Parietal Lobe//Inferior Parietal Lobule
4	794	(−41, −15, 38)	Left Cerebrum//Frontal Lobe//Precentral Gyrus
5	699	(20, −3, 18)	Right Cerebrum//Sub-lobar//Extra-Nuclear

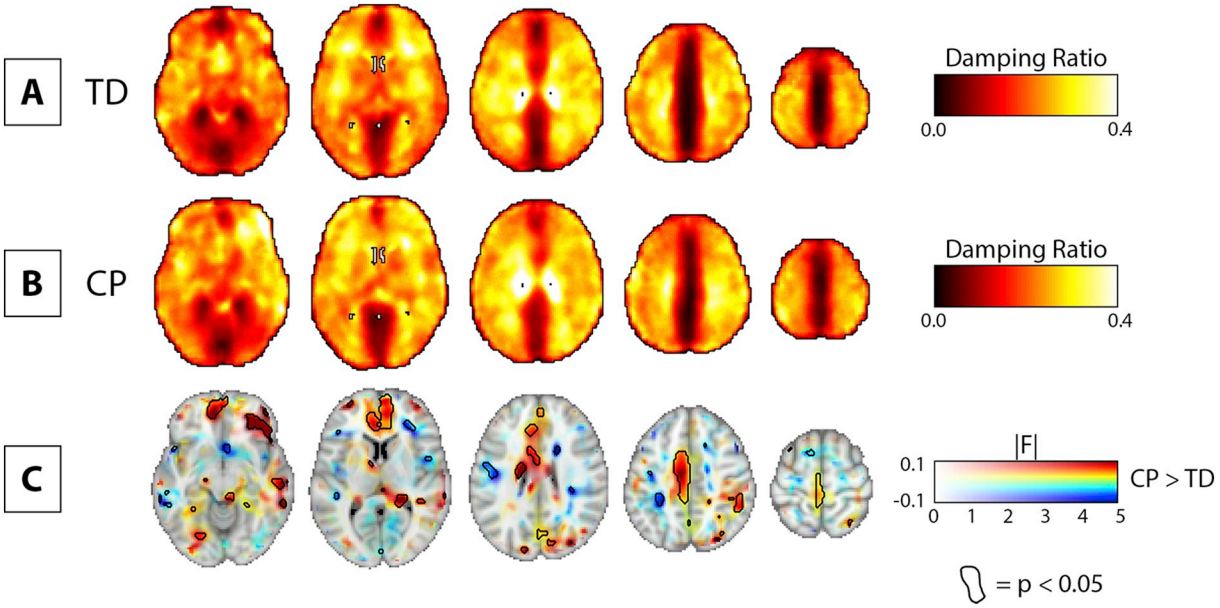

Fig. 5. Voxel-wise comparison of damping ratio between TD and CP groups. A) Example slices of the mean damping ratio map for TD group. B) Example slices of the mean damping ratio map for CP group. C) Multidimensional statistical map including the voxel-wise CP > TD difference map as a colored feature plane; the associated F-statistics in opacity; and areas where $p < 0.05$ circled. 2.0 mm MNI standard-space template underlay for visualization. All images in neurological convention.

Table 4
The five largest clusters of voxels in 2 mm standard space exhibiting significant differences in damping ratio between groups as identified through voxel-wise analysis. MNI coordinates identify the location of the cluster centroid. Note all clusters show significantly higher damping ratio.

Cluster	# Voxels	MNI coordinates	Anatomical location
1	1964	(−25, −41, 44)	Left Cerebrum//Parietal Lobe//Sub-Gyral
2	473	(−17, 22, −9)	Left Cerebrum//Frontal Lobe//Sub-Gyral
3	413	(−3, −18, 4)	Left Cerebrum//Sub-Lobar//Thalamus
4	181	(−1, 16, 47)	Left Cerebrum//Frontal Lobe//Medial Frontal Gyrus
5	158	(−35, 18, 16)	Left Cerebrum//Frontal Lobe//Sub-Gyral

damage in which neuronal cell death occurs in the periventricular WM and results in enlarged lateral ventricles (Lee et al., 2017). We did not include these participants in the group analyses; however, we calculated global stiffness and damping ratio for comparison with the CP group separately, with the large ventricle regions manually removed from ROIs. Interestingly, the two participants exhibited different brain viscoelasticity trends compared to the rest of the CP group: one had even lower cerebral stiffness (female; 8 years; $\mu = 2.65$ kPa and $\xi = 0.277$) while the other had higher (male; 6 years; $\mu = 2.95$ kPa and $\xi = 0.210$). This preliminary observation suggests more research is warranted into how brain mechanical properties are affected by major structural abnormalities in CP.

Damage during neurodevelopment is a slow and quasi-static phenomenon that occurs on the order of weeks or months (Zilles et al., 2013). GM damage is secondary to injury events that occur after 34 weeks of gestation (Flodmark, 2003); given the significant difference in GM viscoelasticity between groups, this may suggest that many of our participants may have experienced such events during that period. Interestingly, we did not observe a significant difference in global WM stiffness or damping ratio between CP and TD. This is potentially due to the heterogeneity of WM and the varying manifestations of CP in our population. To explore whether there were common regions of altered viscoelasticity throughout the brain, we also used a voxel-wise analysis to identify areas showing affected mechanical integrity without making any anatomical *a priori* assumptions.

The voxel-wise analyses resolved large clusters that have significantly lower stiffness in participants with CP, and unexpectedly also revealed areas with higher stiffness. The largest cluster identified by the voxel-wise analysis shows lower stiffness within the left cingulate gyrus and neighboring WM, which spans the frontal and parietal lobes immediately above the corpus callosum. The cingulate gyrus begins its development around the 18th week of gestation (Chi et al., 1977); this region may be affected by a destructive event prior to development, leading to gross malformation of the surrounding area, or a destructive event after development prior to birth, which may reduce integrity of the tissue. The voxel-wise analyses similarly identified several large clusters of higher damping ratio, which additionally suggests reduced brain tissue integrity based on previous studies of cognitive performance and aerobic fitness (Sandroff et al., 2017; Schwarb et al., 2017). Significant clusters did not strongly overlap suggesting independent information to be gained from the two measures.

It is notable that while the children with CP exhibited globally lower stiffness and higher damping ratio, and there were significant clusters of consistently lower and higher properties throughout the brain, the largest clusters had centroids in the left hemisphere potentially indicating greater damage on this side in CP. It is additionally notable that the voxel-wise analysis also identified a cluster with higher stiffness in CP in the right sub-lobar region, which is the fifth largest cluster identified, along with additional smaller clusters with either higher stiffness or lower damping ratio in CP. This could be indicative of a neuroplastic compensatory mechanism that has caused a contralateral increase in stiffness. Such a contralateral effect was previously observed in CP using diffusion tensor imaging (Thomas et al., 2005).

The findings from our two analysis approaches present different yet complementary results. The global ROI analysis identified a decrease in brain tissue stiffness in pediatric CP that was significant in GM only, while the voxel-wise analysis identified decreases and increases in brain tissue stiffness in both GM and WM. The analysis of damping ratio similarly revealed globally higher values in GM, along with significant clusters of both higher and lower values throughout the brain. The majority of brain MRE studies have utilized *a priori* ROIs in examining differences between groups (Hiscox et al., 2016); however, Murphy

et al. recently used a voxel-wise analysis to examine age-dependence in brain stiffness (Murphy et al., 2018). Voxel-wise analyses may be beneficial in examining neuropathological populations like CP where the low specificity of damage to any anatomical brain region in cerebral palsy makes assigning meaningful *a priori* ROIs problematic (Bax, 1964).

Our voxel-wise analyses allowed us to identify more viscoelasticity differences in children with CP because it doesn't require anatomical *a priori* assumptions. As this is the first study on CP using MRE, there are no reliable *a priori* subregions that could be assumed to have affected mechanical integrity. The ROI analysis therefore included only large ROIs (cerebrum and cerebral WM and GM). In this case, adding on a voxel-wise analysis, with estimation of the false discovery rate (FDR) to control for multiple comparisons, complements the ROI analysis by elucidating the specific GM and WM subregions that are particularly affected in CP. Despite the heterogeneity of the CP population, both analyses revealed global and local patterns of altered viscoelasticity that persist across participants, suggesting these regions may be relevant targets for future MRE studies of CP.

There are several limitations to this study. First, we adopted a robust, rapid MRE imaging sequence (single-shot EPI-based) in order to reduce scan time and sensitivity to motion errors in a potentially uncooperative population. However, this required a reduced spatial resolution, limiting our ability to accurately recover mechanical properties in small neuroanatomical ROIs (Johnson et al., 2016). This reduced resolution is expected to result in highly repeatable measures on the order of 1–2% variability based on our recent repeatability measurements in large global regions using the same techniques with higher resolution data (Anderson et al., 2016; Johnson et al., 2016). Second, we enrolled and examined CP participants with only the lowest levels of functional impairment (GMFCS 1 or 2), thus we were unable to observe how mechanical properties of the brain differ with degree of impairment. This choice was made, in part, to improve participant cooperation as all MRI scanning was done in a research setting without sedation. Our population was more cooperative than expected, and future studies may successfully employ a higher resolution MRE imaging sequence, especially if accompanied by an acceleration scheme such as sample interval modulation (SLIM) to reduce total scan time (Klatt et al., 2013, 2015). Given the significant differences observed with only minor disability from CP, we expect future studies examining greater impairment in CP with MRE to potentially find even lower stiffness and higher damping ratio.

5. Conclusion

This is the first study that has examined the mechanical properties of brain tissue in CP, and one of the first brain MRE studies on a pediatric population. Our results suggest that MRE measures are affected in this population even in children at the lowest levels of functional motor impairment. We found significant decreases in the mechanical integrity of brain tissue in the GM and WM of children with CP, as well as some significant increases in other areas possibly representing compensatory mechanisms. In future studies, brain tissue viscoelasticity measured with MRE could be used to aid diagnosis or evaluation of CP, elucidate how brain structure relates to functional or clinical outcome measures in CP, or how therapeutic interventions affect neuroplastic repair and recovery in this population.

Acknowledgements

This work is supported by the Delaware INBRE program with a grant from the National Institutes of General Medical Sciences (P20-GM103446) from the National Institutes of Health and the State of Delaware.

Appendix A. Supplementary data

Supplementary data to this article can be found online at https://doi.org/10.1016/j.nicl.2019.101750.

References

Aisen, M.L., Kerkovich, D., Mast, J., Mulroy, S., Wren, T.A.L., Kay, R.M., Rethlefsen, S.A., 2017. Cerebral palsy: clinical care and neurological rehabilitation. Lancet Neurol. 10, 844–852. https://doi.org/10.1016/S1474-4422(11)70176-4.

Allen, E.A., Erhardt, E.B., Calhoun, V.D., 2012. Data visualization in the neurosciences: overcoming the curse of dimensionality. Neuron 74, 603–608. https://doi.org/10.1016/j.neuron.2012.05.001.

Anderson, A.T., Van Houten, E.E.W., McGarry, M.D.J., Paulsen, K.D., Holtrop, J.L., Sutton, B.P., Georgiadis, J.G., Johnson, C.L., 2016. Observation of direction-dependent mechanical properties in the human brain with multi-excitation MR elastography. J. Mech. Behav. Biomed. Mater. 59, 538–546. https://doi.org/10.1016/j.jmbbm.2016.03.005.

Arani, A., Murphy, M.C., Glaser, K.J., Manduca, A., Lake, D.S., Kruse, S.A., Jack, C.R., Ehman, R.L., Huston, J., 2015. Measuring the effects of aging and sex on regional brain stiffness with MR elastography in healthy older adults. Neuroimage 111, 59–64. https://doi.org/10.1016/j.neuroimage.2015.02.016.

Bax, M., 1964. Terminology and classification of cerebral palsy. Dev. Med. Child Neurol. 6, 295–297. https://doi.org/10.1111/j.1469-8749.1964.tb10791.x.

Bax, M., Goldstein, M., Rosenbaum, P., Leviton, A., Paneth, N., Dan, B., Jacobsson, B., Damiano, D., 2005. Proposed definition and classification of cerebral palsy, April 2005 (executive Committee for the Definition of cerebral palsy). Dev. Med. Child Neurol. 47, 571–576. https://doi.org/10.1017/S001216220500112X.

Benjamini, Y., Benjamini, Y.H., Hochberg, Y., 1995. Controlling the false discovery rate: a practical and powerful approach to multiple testing. J. R. Stat. Soc. Ser. B 289–300.

Chi, J.G., Dooling, E.C., Gilles, F.H., 1977. Gyral development of the human brain. Ann. Neurol. 1, 86–93. https://doi.org/10.1002/ana.410010109.

ElSheikh, M., Arani, A., Perry, A., Boeve, B.F., Meyer, F.B., Savica, R., Ehman, R.L., Huston, J., 2017. MR Elastography demonstrates unique regional brain stiffness patterns in dementias. Am. J. Roentgenol. 209, 403–408. https://doi.org/10.2214/AJR.16.17455.

Fehlner, A., Behrens, J.R., Streitberger, K., Papazoglou, S., Bellmann-strobl, J., Ruprecht, K., Sack, I., 2016. Higher-resolution MR Elastography reveals early mechanical signatures of Neuroinflammation in patients with clinically isolated syndrome. J. Magn. Reson. Imaging 44, 51–58. https://doi.org/10.1002/jmri.25129.

Flodmark, O., 2003. Brain imaging studies of individuals with cerebral palsy. Riv. Neuroradiol. 16, 183–184. https://doi.org/10.1177/1971400903016SP244.

Gosling, A.S., 2017. Recent advances in the neuroimaging and neuropsychology of cerebral palsy. Appl. Neuropsychol. Child 6, 55–63.

Himmelmann, K., Horber, V., De La Cruz, J., Horridge, K., Mejaski-Bosnjak, V., Hollody, K., Krägeloh-Mann, I., Group, the S.W, 2017. MRI classification system (MRICS) for children with cerebral palsy: development, reliability, and recommendations. Dev. Med. Child Neurol. 59, 57–64. https://doi.org/10.1111/dmcn.13166.

Hiscox, L.V., Johnson, C.L., Barnhill, E., McGarry, M.D.J., Huston, J., Van Beek, E.J.R., Starr, J.M., Roberts, N., 2016. Magnetic resonance elastography (MRE) of the human brain: technique, findings and clinical applications. Phys. Med. Biol. 61, R401–R437. https://doi.org/10.1088/0031-9155/61/24/R401.

Hiscox, L.V., Johnson, C.L., McGarry, M.D.J., Perrins, M., Littlejohn, A., van Beek, E.J.R., Roberts, N., Starr, J.M., 2018. High-resolution magnetic resonance elastography reveals differences in subcortical gray matter viscoelasticity between young and healthy older adults. Neurobiol. Aging 65, 158–167. https://doi.org/10.1016/j.neurobiolaging.2018.01.010.

Jenkinson, M., 2003. Fast, automated, N-dimensional phase-unwrapping algorithm. Magn. Reson. Med. 49, 193–197. https://doi.org/10.1002/mrm.10354.

Jenkinson, M., Smith, S., 2001. A global optimisation method for robust affine registration of brain images. Med. Image Anal. 5, 143–156. https://doi.org/10.1016/S1361-8415(01)00036-6.

Jenkinson, M., Bannister, P.R., Brady, M., Smith, S.M., 2002. Improved optimization for the robust and accurate linear registration and motion correction of brain images. Neuroimage 17, 825–841. https://doi.org/10.1006/nimg.2002.1132.

Johnson, C.L., Telzer, E.H., 2018. Magnetic resonance elastography for examining developmental changes in the mechanical properties of the brain. Dev. Cogn. Neurosci. 33, 176–181. https://doi.org/10.1016/j.dcn.2017.08.010.

Johnson, C.L., Schwarb, H., McGarry, M.D.J., Anderson, A.T., Huesmann, G.R., Sutton, B.P., Cohen, N.J., 2016. Viscoelasticity of subcortical gray matter structures. Hum. Brain Mapp. 37, 4221–4233. https://doi.org/10.1002/hbm.23314.

Johnson, C.L., Schwarb, H., Horecka, K.M., McGarry, M.D.J., Hillman, C.H., Kramer, A.F., Cohen, N.J., Barbey, A.K., 2018. Double dissociation of structure-function relationships in memory and fluid intelligence observed with magnetic resonance elastography. Neuroimage 171, 99–106. https://doi.org/10.1016/j.neuroimage.2018.01.007.

Klatt, D., Yasar, T.K., Royston, T.J., Magin, R.L., 2013. Sample interval modulation for the simultaneous acquisition of displacement vector data in magnetic resonance elastography: theory and application. Phys. Med. Biol. 58, 8663–8675. https://doi.org/10.1088/0031-9155/58/24/8663.

Klatt, D., Johnson, C.L., Magin, R.L., 2015. Simultaneous, multidirectional acquisition of displacement fields in magnetic resonance elastography of the in vivo human brain. J. Magn. Reson. Imaging 42, 297–304. https://doi.org/10.1002/jmri.24806.

Korzeniewski, S.J., Birbeck, G., DeLano, M.C., Potchen, M.J., Paneth, N., 2007. A

systematic review of neuroimaging for cerebral palsy. J. Child Neurol. 23, 216–227. https://doi.org/10.1177/0883073807307983.
Krigger, K.W., 2006. Cerebral palsy : an overview. Am. Fam. Physician 73, 91–100.
Lee, D., Pae, C., Lee, J.D., Park, E.S., Cho, S.-R., Um, M.-H., Lee, S.-K., Oh, M.-K., Park, H.-J., 2017. Analysis of structure–function network decoupling in the brain systems of spastic diplegic cerebral palsy. Hum. Brain Mapp. 38, 5292–5306. https://doi.org/10.1002/hbm.23738.
Maldjian, J.A., Laurienti, P.J., Kraft, R.A., Burdette, J.H., 2003. An automated method for neuroanatomic and cytoarchitectonic atlas-based interrogation of fMRI data sets. Neuroimage 19, 1233–1239. https://doi.org/10.1016/S1053-8119(03)00169-1.
Manduca, A., Oliphant, T.E., Dresner, M.A., Mahowald, J.L., Kruse, S.A., Amromin, E., Felmlee, J.P., Greenleaf, J.F., Ehman, R.L., 2001. Magnetic resonance Elastography: non-invasive mapping of tissue elasticity. Med. Image Anal. 5, 237–254.
McGarry, M.D.J., Van Houten, E.E.W., 2008. Use of a Rayleigh damping model in elastography. Med. Biol. Eng. Comput. 46, 759–766. https://doi.org/10.1007/s11517-008-0356-5.
McGarry, M.D.J., Van Houten, E.E.W., Johnson, C.L., Georgiadis, J.G., Sutton, B.P., Weaver, J.B., Paulsen, K.D., 2012. Multiresolution MR elastography using nonlinear inversion. Med. Phys. 39, 6388–6396. https://doi.org/10.1118/1.4754649.
McIlvain, G., Schwarb, H., Cohen, N.J., Telzer, E.H., Johnson, C.L., 2018. Mechanical properties of the in vivo adolescent human brain. Dev. Cogn. Neurosci. 34, 27–33. https://doi.org/10.1016/j.dcn.2018.06.001.
Murphy, M.C., Huston, J., Ehman, R.L., 2017. MR elastography of the brain and its application in neurological diseases. Neuroimage. https://doi.org/10.1016/j.neuroimage.2017.10.008.
Murphy, M.C., Manduca, A., Trzasko, J.D., Glaser, K.J., Huston, J., Ehman, R.L., 2018. Artificial neural networks for stiffness estimation in magnetic resonance elastography. Magn. Reson. Med. 80, 351–360. https://doi.org/10.1002/mrm.27019.
Muthupillai, R., Lomas, D.J., Rossman, P.J., Greenleaf, J.F., Manduca, A., Ehman, R.L., 1995. Magnetic resonance elastography by direct visualization of propagating acoustic strain waves. Science 269, 1854–1857 (80-.).
Nagae, L.M., Hoon, A.H., Stashinko, E., Lin, D., Zhang, W., Levey, E., Wakana, S., Jiang, H., Leite, C.C., Lucato, L.T., van Zijl, P.C.M., Johnston, M.V., Mori, S., 2007. Diffusion tensor imaging in children with periventricular Leukomalacia: variability of injuries to white matter tracts. Am. J. Neuroradiol. 28, 1213 LP–1222.
Robinson, M.N., Peake, L.J., Ditchfield, M.R., Reid, S.M., Lanigan, A., Reddihough, D.S., 2009. Magnetic resonance imaging findings in a population-based cohort of children with cerebral palsy. Dev. Cogn. Neurosci. 51, 39–45. https://doi.org/10.1111/j.1469-8749.2008.03127.x.
Sack, I., Jöhrens, K., Wuerfel, J., Braun, J., 2013. Structure-sensitive elastography: on the viscoelastic powerlaw behavior of in vivo human tissue in health and disease. Soft Matter 9, 5672–5680. https://doi.org/10.1039/c3sm50552a.
Sandroff, B.M., Johnson, C.L., Motl, R.W., 2017. Exercise training effects on memory and hippocampal viscoelasticity in multiple sclerosis: a novel application of magnetic resonance elastography. Neuroradiology 59, 61–67. https://doi.org/10.1007/s00234-016-1767-x.
Schwarb, H., Johnson, C.L., McGarry, M.D.J., Cohen, N.J., 2016. Medial temporal lobe viscoelasticity and relational memory performance. Neuroimage 132, 534–541. https://doi.org/10.1016/j.neuroimage.2016.02.059.
Schwarb, H., Johnson, C.L., Daugherty, A.M., Hillman, C.H., Kramer, A.F., Cohen, N.J., Barbey, A.K., 2017. Aerobic fitness, hippocampal viscoelasticity, and relational memory performance. Neuroimage 153, 179–188. https://doi.org/10.1016/j.neuroimage.2017.03.061.
Simes, J., 1986. An improved Bonferroni procedure for multiple tests of significance. Biometrika. https://doi.org/10.1093/biomet/73.3.751.
Thomas, B., Eyssen, M., Peeters, R., Molenaers, G., Van Hecke, P., De Cock, P., Sunaert, S., 2005. Quantitative diffusion tensor imaging in cerebral palsy due to periventricular white matter injury. Brain 128, 2562–2577.
Zhang, Y., Brady, M., Smith, S., 2001. Segmentation of brain MR images through a hidden Markov random field model and the expectation-maximization algorithm. IEEE Trans. Med. Imaging 20, 45–57. https://doi.org/10.1109/42.906424.
Zilles, K., Palomero-Gallagher, N., Amunts, K., 2013. Development of cortical folding during evolution and ontogeny. Trends Neurosci. 36, 275–284. https://doi.org/10.1016/j.tins.2013.01.006.